On the possibility to detect multipolar order in URu_{2}Si_{2} by the electric quadrupolar transition of resonant elastic x-ray scattering

Y. L. Wang, G. Fabbris, D. Meyers, N. H. Sung, R. E. Baumbach, E. D. Bauer, P. J. Ryan, J.-W. Kim, X. Liu, M. P. M. Dean, G. Kotliar, and X. Dai

Phys. Rev. B **96**, 085146 — Published 30 August 2017

DOI: 10.1103/PhysRevB.96.085146

On the possibility to detect multipolar order in URu_2Si_2 by the electric quadrupolar transition of resonant elastic X-ray scattering

Y. L. Wang,[1] G. Fabbris,[1] D. Meyers,[1] N. H. Sung,[2] R. E. Baumbach,[2,3] E. D. Bauer,[2] P. J. Ryan,[4,5] J.-W. Kim,[4] X. Liu,[6] M. P. M. Dean,[1] G. Kotliar,[1,7] and X. Dai[6]

[1]*Department of Condensed Matter Physics and Materials Science, Brookhaven National Laboratory, Upton, New York 11973, USA*
[2]*Materials Physics and Applications Division, Los Alamos National Laboratory, Los Alamos, New Mexico 87545, USA*
[3]*Condensed Matter Group, National High Magnetic Field Laboratory, Florida State University, Tallahassee, Florida 32310, USA*
[4]*Advanced Photon Source, Argonne National Laboratory, Argonne, Illinois 60439, USA*
[5]*School of Physical Sciences, Dublin City University, Dublin 9, Ireland*
[6]*Beijing National Laboratory for Condensed Matter Physics and Institute of Physics, Chinese Academy of Sciences, Beijing 100190, China*
[7]*Department of Physics and Astronomy, Rutgers University, Piscataway, New Jersey 08856, USA*

(Dated: August 16, 2017)

Resonant elastic X-ray scattering is a powerful technique for measuring multipolar order parameters. In this paper, we theoretically and experimentally study the possibility of using this technique to detect the proposed multipolar order parameters in URu_2Si_2 at the U-L_3 edge with the electric quadrupolar transition. Based on an atomic model, we calculate the azimuthal dependence of the quadrupolar transition at the U-L_3 edge. The results illustrate the potential of this technique for distinguishing different multipolar order parameters. We then perform experiments on ultra-clean single crystals of URu_2Si_2 at the U-L_3 edge to search for the predicted signal, but do not detect any indications of multipolar moments within the experimental uncertainty. We theoretically estimate the orders of magnitude of the cross-section and the expected count rate of the quadrupolar transition and compare them to the dipolar transitions at the U-M_4 and U-L_3 edges, clarifying the difficulty in detecting higher order multipolar order parameters in URu_2Si_2 in the current experimental setup.

I. INTRODUCTION

The heavy fermion compound URu_2Si_2 undergoes a phase transition at $T_{HO} = 17.5$ K to the so called "Hidden Order" (HO) phase, in which the sharp discontinuous specific heat signals a clear second-order phase transition[1]. Earlier studies based on neutron scattering[2,3] and muon spin rotation[4] conclude that it is a phase transition to type-I antiferromagnet (AFM) with the ordered moment polarized along the tetragonal c-axis. However, the observed ordered moment is anomalously very small ($\sim 0.04 \pm 0.01\mu_B$)[2–4], which cannot account for the observed large entropy loss ($\sim 0.2R\ln 2$), and the primary order parameter (OP) is unlikely to be magnetic dipole. Further high pressure experiments on URu_2Si_2 find a first-order phase transition from the HO phase to a large moment antiferromagnetic (LMAF) phase[5–7]. These findings further indicate that the HO phase is distinct from the LMAF and the primary OP should be some complex object which is different from a magnetic dipole.

Theoretically, many different schemes of OPs have been proposed, such as multipolar order[8–18], charge- or spin-density wave[19–22], chiral spin state[23], orbital antiferromagnetism[24], helicity order[25], dynamic symmetry breaking[26], nematic order[27], hybridization wave[28], and hastatic order[29,30]. However, through 30 years of efforts, there is still a lack of convincing evidence to uncover the HO mystery. For a more complete review of the theoretical and experimental progress, see Ref.[31,32].

Among the many proposals of OPs, the multipolar order is a promising candidate. Recently, Raman scattering experiments[33–35] find a sharp low energy excitation with A_{2g} symmetry below T_{HO}. Further analysis[34,35] indicates that this A_{2g} excitation is consistent with the hexadecapolar order proposed by Haule and Kotliar[14]. However, these Raman scattering experiments provide indirect information about the ground state in the sense that they cannot measure modes at the ordering wavevector. Wavevector-resolved techniques are desirable to make more definitive conclusions. Among the many options, resonant elastic X-ray scattering (REXS) is a powerful tool to directly detect the order of electrons including complex spin and charge multipoles[36,37]. There have been already a few REXS experiments[38–41] performed to identify the multipolar order in the HO phase of URu_2Si_2. Amitsuka *et al.*[40] and Walker *et al.*[41] performed REXS experiments at the U-M_4 ($3d_{3/2} \rightarrow 5f$) edge below T_{HO} and their results have excluded the possibility of any quadrupolar OPs. However, the M_4 edge involves electric dipolar transitions (E1) and has minimal sensitivity to multipoles with a rank larger than 2. The electric quadrupolar transition (E2) can be used to detect octupole and hexadecapole, but unfortunately, the intensity of E2 is usually much weaker than that of E1.

Recently, dos Reis *et al.*[42] discussed a sizable E2 contribution to the U-$L_{2,3}$ X-ray magnetic circular dichroism (XMCD) signal in their study of U compounds. The en-

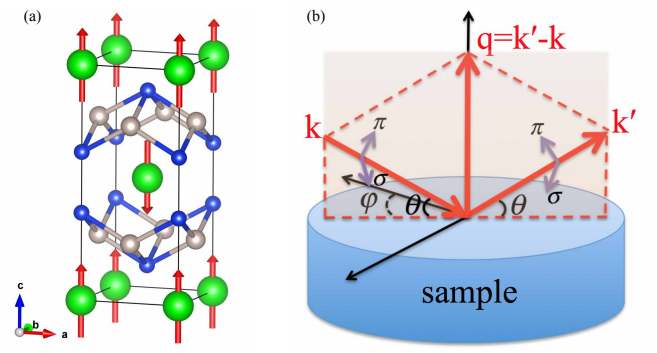

FIG. 1. (Color online). (a) The crystal structure of URu_2Si_2. We assume a type-I antiferro-multipolar order on Uranium sites. (b) Illustration of experimental setup. A beam of polarized x-rays $\boldsymbol{k}$ is incident on the [001] sample face with an angle θ and scattered by electrons, and then the scattered x-rays $\boldsymbol{k}'$ with outgoing angle θ and specific polarization is analyzed. φ is the azimuthal angle. For linear polarization, π (σ) polarization is parallel (normal) to the scattering plane.

hanced E2 signal may be due to the large wavevector k (10.615 $\mathring{A}^{-1}$ and 8.699 $\mathring{A}^{-1}$) at $L_{2,3}$ edges which means that the term $i\boldsymbol{k}\cdot\boldsymbol{r}$ in the expansion of $e^{i\boldsymbol{k}\cdot\boldsymbol{r}}$ cannot be ignored. This unexpected finding provides a promising hope to use the E2 transition to directly detect multipolar OPs in URu_2Si_2.

In this paper, we theoretically and experimentally study the possibility to detect the proposed multipolar OPs in URu_2Si_2 via E2 transition of REXS. Based on an atomic model, we first calculate the azimuthal dependences to show that it can identify different multipolar OPs by symmetry. Then, we do REXS experiments on ultra-clean sample of URu_2Si_2 single crystal to search for the possible signal of multipolar OPs. Finally, we justify the experimental results by theoretically estimating the relative strength of E2 transition at L_3 edge (L_3-$E2$) compared with E1 transition at M_4 edge (M_4-$E1$) and L_3 edge ($2p_{3/2} \rightarrow 6d$, L_3-$E1$), and the expected flux of the scattered photons.

II. METHODS

A. Atomic calculations

Fig. 1(a) is the crystal structure of URu_2Si_2, which has a body-centered tetragonal structure. In the present study, we assume a type-I antiferro-multipolar order on U sites, where sublattice A: U$(0,0,0)$ and sublattice B: U$(0.5,0.5,0.5)$ have opposite signs of the expectation value of the multipolar moment. The ordering wavevector is $Q_{\rm AF}=(0,0,1)$. Fig. 1(b) is a typical experimental setup of REXS. A beam of polarized X-ray $\boldsymbol{k}$ is incident on the sample with an angle θ and then the scattered X-ray $\boldsymbol{k}'$ with outgoing angle θ and specific polarization is analyzed. The double-differential cross section[36] for REXS is,

$$\frac{\mathrm{d}^2\sigma}{\mathrm{d}\Omega \mathrm{d}E} = r_e^2 m^2 \omega_{k'}^3 \omega_k \left|\mathcal{F}_{gg}\left(\boldsymbol{k},\boldsymbol{k}',\hbar\omega_k,\hbar\omega_{k'},\boldsymbol{\epsilon},\boldsymbol{\epsilon}'\right)\right|^2, \quad (1)$$

where, $r_e = e^2/(4\pi\epsilon_0 mc^2)$ is the classical electron radius, $\mathcal{F}_{gg}$ is the scattering amplitude at zero temperature,

$$\mathcal{F}_{gg}\left(\boldsymbol{k},\boldsymbol{k}',\hbar\omega_k,\hbar\omega_{k'},\boldsymbol{\epsilon},\boldsymbol{\epsilon}'\right) = \sum_n \frac{\left\langle g\left|\hat{\mathcal{D}}'^{\dagger}\right|n\right\rangle\left\langle n\left|\hat{\mathcal{D}}\right|g\right\rangle}{\hbar\omega_k + E_g - E_n + i\Gamma/2}, \quad (2)$$

where, $\boldsymbol{k}$ is the incoming light with energy $\hbar\omega_k$ and polarization $\boldsymbol{\epsilon}$, $\boldsymbol{k}'$ is the outgoing light with energy $\hbar\omega_{k'}$ and polarization $\boldsymbol{\epsilon}'$, and $\boldsymbol{q}=\boldsymbol{k}'-\boldsymbol{k}$ is the scattering vector. $|g\rangle, E_g$ is the ground state and $|n\rangle, E_n$ is the eigenstate of the intermediate Hamiltonian including a core-hole. Γ is the lifetime width of the core hole. For U, $\Gamma \approx 8$ eV at the L_3 edge and $\Gamma \approx 3.5$ eV at the M_4 edge. $\hat{\mathcal{D}}$ and $\hat{\mathcal{D}}'^{\dagger}$ are the transition operators for absorption and emission processes,

$$\begin{aligned}\hat{\mathcal{D}} &= \boldsymbol{P}^{(m)}\cdot\sum_{\boldsymbol{R}}\hat{\boldsymbol{D}}_{\boldsymbol{R}}^{(m)} \\ &= \boldsymbol{P}^{(m)}\cdot\left(\sum_{\boldsymbol{R}} e^{i\boldsymbol{k}\cdot\boldsymbol{R}}\sum_i \hat{\boldsymbol{r}}_{\boldsymbol{R},i}^{(m)}\right), \quad (3)\\ \hat{\mathcal{D}}'^{\dagger} &= \boldsymbol{P}^{(m)\prime\star}\cdot\sum_{\boldsymbol{R}}\hat{\boldsymbol{D}}_{\boldsymbol{R}}^{(m)\dagger} \\ &= \boldsymbol{P}^{(m)\prime\star}\cdot\left(\sum_{\boldsymbol{R}} e^{-i\boldsymbol{k}'\cdot\boldsymbol{R}}\sum_i \hat{\boldsymbol{r}}_{\boldsymbol{R},i}^{(m)\dagger}\right) \quad (4)\end{aligned}$$

where, $\boldsymbol{R}$ is the site index, i is the index of electron that is bound to site $\boldsymbol{R}$. $\boldsymbol{P}^{(m)}$ is a rank-m tensor for geometry part including polarization and wavevector of photon, $\hat{\boldsymbol{r}}^{(m)}$ is a single particle rank-m tensor operator of electron.

For E1-E1 transition,

$$\boldsymbol{P}^{(1)}\cdot\hat{\boldsymbol{r}}^{(1)} = \epsilon_x\hat{x}+\epsilon_y\hat{y}+\epsilon_z\hat{z}, \quad (5)$$
$$\boldsymbol{P}^{(1)\prime\star}\cdot\hat{\boldsymbol{r}}^{(1)\dagger} = \epsilon_x'^{\star}\hat{x}+\epsilon_y'^{\star}\hat{y}+\epsilon_z'^{\star}\hat{z}. \quad (6)$$

For E2-E2 transition[43],

$$(\hat{\boldsymbol{r}}^{(2)})_1 = \frac{\sqrt{3}}{2}(\hat{x}^2-\hat{y}^2), \quad (7)$$
$$(\hat{\boldsymbol{r}}^{(2)})_2 = \frac{1}{2}(3\hat{z}^2-\hat{r}^2), \quad (8)$$
$$(\hat{\boldsymbol{r}}^{(2)})_3 = \sqrt{3}\hat{y}\hat{z}, \quad (9)$$
$$(\hat{\boldsymbol{r}}^{(2)})_4 = \sqrt{3}\hat{z}\hat{x}, \quad (10)$$
$$(\hat{\boldsymbol{r}}^{(2)})_5 = \sqrt{3}\hat{x}\hat{y}, \quad (11)$$

and

$$\boldsymbol{P}_1^{(2)} = \frac{k}{3}\frac{\sqrt{3}}{2}(\epsilon_x\tilde{k}_x - \epsilon_y\tilde{k}_y), \tag{12}$$

$$\boldsymbol{P}_2^{(2)} = \frac{k}{3}\frac{1}{2}(2\epsilon_z\tilde{k}_z - \epsilon_x\tilde{k}_x - \epsilon_y\tilde{k}_y), \tag{13}$$

$$\boldsymbol{P}_3^{(2)} = \frac{k}{3}\frac{\sqrt{3}}{2}(\epsilon_y\tilde{k}_z + \epsilon_z\tilde{k}_y), \tag{14}$$

$$\boldsymbol{P}_4^{(2)} = \frac{k}{3}\frac{\sqrt{3}}{2}(\epsilon_z\tilde{k}_x + \epsilon_x\tilde{k}_z), \tag{15}$$

$$\boldsymbol{P}_5^{(2)} = \frac{k}{3}\frac{\sqrt{3}}{2}(\epsilon_x\tilde{k}_y + \epsilon_y\tilde{k}_x). \tag{16}$$

where, k and $\tilde{\boldsymbol{k}}$ are the length and direction of the wavevector, respectively. We assume the absorption and emission process take place at the same site, then the scattering amplitude can be written as,

$$\mathcal{F}_{gg} \propto \sum_{\boldsymbol{R}} e^{-i\boldsymbol{q}\cdot\boldsymbol{R}} F_{gg}^{\boldsymbol{R}}, \tag{17}$$

with

$$F_{gg}^{\boldsymbol{R}} = \sum_n \frac{\left\langle g \left| \hat{\mathcal{D}}_{\boldsymbol{R}}^\dagger \right| n \right\rangle \left\langle n \left| \hat{\mathcal{D}}_{\boldsymbol{R}} \right| g \right\rangle}{\hbar\omega_{\boldsymbol{k}} + E_g - E_n + i\Gamma/2}. \tag{18}$$

where $\hat{\mathcal{D}}_{\boldsymbol{R}} = \boldsymbol{P}^{(m)} \cdot \hat{\boldsymbol{D}}_{\boldsymbol{R}}^{(m)}$ and $\hat{\mathcal{D}}_{\boldsymbol{R}}^\dagger = \boldsymbol{P}^{(m)\prime\star} \cdot \hat{\boldsymbol{D}}_{\boldsymbol{R}}^{(m)\dagger}$.

We further make single atom approximation, i.e., approximating the states $|g\rangle$ and $|n\rangle$ as single atomic states. Then the total scattering amplitude can be written as the summation of the contributions from two sublattices A and B of U atoms,

$$\mathcal{F}_{gg} \propto \sum_{\boldsymbol{R}_A} e^{-i\boldsymbol{q}\cdot\boldsymbol{R}_A} F_{gg}^{\boldsymbol{R}_A} + \sum_{\boldsymbol{R}_B} e^{-i\boldsymbol{q}\cdot\boldsymbol{R}_B} F_{gg}^{\boldsymbol{R}_B}, \tag{19}$$

where,

$$F_{gg}^{\boldsymbol{R}_A} = \sum_n \frac{\left\langle g^A \left| \hat{\mathcal{D}}_{\boldsymbol{R}_A}^\dagger \right| n^A \right\rangle \left\langle n^A \left| \hat{\mathcal{D}}_{\boldsymbol{R}_A} \right| g^A \right\rangle}{\hbar\omega_k + E_{g^A} - E_{n^A} + i\Gamma/2}, \tag{20}$$

$$F_{gg}^{\boldsymbol{R}_B} = \sum_n \frac{\left\langle g^B \left| \hat{\mathcal{D}}_{\boldsymbol{R}_B}^\dagger \right| n^B \right\rangle \left\langle n^B \left| \hat{\mathcal{D}}_{\boldsymbol{R}_B} \right| g^B \right\rangle}{\hbar\omega_k + E_{g^B} - E_{n^B} + i\Gamma/2}. \tag{21}$$

$\left|g^A\right\rangle$ ($\left|n^A\right\rangle$) and $\left|g^B\right\rangle$ ($\left|n^B\right\rangle$) are the ground (intermediate) states of U atoms A and B, respectively. In calculation, we choose the ground states to induce opposite signs of the expectation value of multipolar moment at the A and B site.

We use the Cowan-Butler-Thole approach[44–47] to exactly diagonalize the atomic Hamiltonian for ground and excited configurations and then get the transition matrix. For URu_2Si_2, we assume a $5f^2$ ground configuration. For M_4-$E1$, L_3-$E1$ and L_3-$E2$ transitions, the excited configurations are $3d^5 5f^3$, $2p^5 5f^2 6d^1$ and $2p^5 5f^3$, respectively. The Slater integrals F^k, G^k and spin-orbit coupling (SOC) ζ of the valence and core electrons are calculated by the Hartree-Fock (HF) methods in Cowan's code[44]. Usually, HF will overestimate them, so we rescale F^k, G^k by 80% and rescale SOC ζ by 92% for $2p$ core hole and 96% for $3d$ core hole, respectively. The parameters are listed in the Appendix.

According to Hund's rule coupling, the $5f^2$ configuration has a ground state with total angular momentum $J = 4$ under $SO(3)$ symmetry. With D_{4h} crystalline electric field (CEF) symmetry, these nine ground state will split into five singlets and two doublets[17,48],

$$\left|A_{1g}^{(1)}(\alpha)\right\rangle = \cos\alpha\,|0\rangle + \frac{\sin\alpha}{\sqrt{2}}\left(|4\rangle + |-4\rangle\right), \tag{22}$$

$$\left|A_{1g}^{(2)}(\alpha)\right\rangle = \sin\alpha\,|0\rangle - \frac{\cos\alpha}{\sqrt{2}}\left(|4\rangle + |-4\rangle\right), \tag{23}$$

$$|A_{2g}\rangle = \frac{i}{\sqrt{2}}\left(|4\rangle - |-4\rangle\right), \tag{24}$$

$$|B_{1g}\rangle = \frac{1}{\sqrt{2}}\left(|2\rangle + |-2\rangle\right), \tag{25}$$

$$|B_{2g}\rangle = \frac{i}{\sqrt{2}}\left(|2\rangle - |-2\rangle\right), \tag{26}$$

$$\left|E_g^{(1)}(\beta)\right\rangle = \cos\beta\,|\mp 1\rangle + \sin\beta\,|\pm 3\rangle, \tag{27}$$

$$\left|E_g^{(2)}(\beta)\right\rangle = \sin\beta\,|\mp 1\rangle - \cos\beta\,|\pm 3\rangle. \tag{28}$$

In Ref.[17], the authors list the definition of the multipole up to rank-5. We will follow this definition in the present paper and only discuss multipole up to rank-4 that can, in principle, be detected via the $E2$ transition. We build different ground states which will induce dipole, quadrupole, octupole and hexadecapole orders.

The ground state that will induce $A_{2+}(A_{2-})$ order can be constructed by a linear combination of $|A_{2g}\rangle$ and $\left|A_{1g}^{(2)}\right\rangle$,

$$\left|g^{A(B)}\right\rangle = \frac{1}{\sqrt{2}}\left(|A_{2g}\rangle \pm e^{i\eta}\left|A_{1g}^{(2)}(40^o)\right\rangle\right), \tag{29}$$

where, we take plus sign for $\left|g^A\right\rangle$ and minus sign for $\left|g^B\right\rangle$. Note that the subscript $+(-)$ in $A_{2+}(A_{2-})$ means time-reversal even (odd). When $\eta = 0$, it will induce a A_{2+} hexadecapolar order $H_z^\alpha = \frac{\sqrt{35}}{2}\overline{J_x J_y (J_x^2 - J_y^2)}$, while $\eta = \pi/2$, it will induce a A_{2-} dipolar order J_z and octupolar order $T_z^\alpha = \frac{1}{2}\overline{J_z(5J_z^2 - 3J^2)}$. This scheme is proposed by Haule and Kotliar[14] by a LDA+DMFT calculation. In their LDA+DMFT calculation, they also figure out α in $A_{1g}^{(2)}$ should be about 40°. H_z^α is proposed to be the primary OP in the HO phase. It can be also induced as a secondary OP in the hastatic order scheme[30].

The ground state that will induce $B_{1+}(B_{1-})$ order can be written as,

$$\left|g^{A(B)}\right\rangle = \frac{1}{\sqrt{2}}\left(|B_{1g}\rangle \pm e^{i\eta}\left|A_{1g}^{(2)}(40^o)\right\rangle\right), \tag{30}$$

When $\eta = 0$, it will induce a B_{1+} quadrupolar order[10] $O_{22} = \frac{\sqrt{3}}{2}\overline{J_x^2 - J_y^2}$ and hexadecapolar order $O_{42} =$

$\frac{\sqrt{5}}{4}\overline{(J_x^2-J_y^2)(7J_z^2-J^2)}$, while $\eta=\pi/2$ it will induce a B_{1-} octupolar order[12] $T_{xyz}=\sqrt{15}\overline{J_xJ_yJ_z}$.

The ground state that will induce $B_{2+}(B_{2-})$ order can be written as,

$$\left|g^{A(B)}\right\rangle=\frac{1}{\sqrt{2}}\left(|B_{2g}\rangle\pm e^{i\eta}\left|A_{1g}^{(2)}(40^o)\right\rangle\right), \tag{31}$$

when $\eta=0$ it will induce a B_{2+} quadrupolar order[10] $O_{xy}=\sqrt{3}\overline{J_xJ_y}$ and hexadecapolar order $H_z^\beta=\frac{\sqrt{5}}{2}\overline{J_xJ_y(7J_z^2-J^2)}$, while $\eta=\pi/2$, it will induce a B_{2-} octupolar order[12] $T_z^\beta=\frac{\sqrt{15}}{2}\overline{J_z(J_x^2-J_y^2)}$.

B. REXS Experiment

URu_2Si_2 samples were grown using the Czocharalski method[49]. The residual resistivity ratio (RRR) was measured in various pieces of sample; the REXS experiment was performed on the sample with highest RRR (= 361). REXS measurements were performed across the U L_3 edge ($\approx$ 17.21 keV) at the 6-ID-B beamline of the Advanced Photon Source at Argonne National Laboratory. The sample was glued to a Cu holder using GE varnish. The holder was placed inside a Be dome filled with He gas, which in turn was mounted on the cold finger of a He closed cycle cryostat. A six circle diffractometer was used to move through reciprocal space. Measurements were performed using a scintillator point detector with 1×1 mm^2 slits. Tetragonal notation with $a=b=4.108$ Å and $c=9.514$ Å is used throughout the paper.

III. RESULTS AND DISCUSSION

A. Azimuthal dependence for different multipolar order parameters

In REXS experiment, azimuthal measurements are used to identify the symmetry of the underlying OPs. Although Nagao *et al.*[43] have figured out the analytic formula of the azimuthal dependences for $E2$ transition, we still explicitly calculate and plot the azimuthal dependences to show the symmetry difference for different multipolar OPs. The results for a $(0,0,3)$ reflection are plotted in Fig. 2. For each multipolar OP, both $\sigma\pi$ and $\sigma\sigma$ channels are plotted, and their intensity is normalized by the maximum of the $\sigma\pi$ channel. Fig. 2(a,b) plots the results of the A_{2+} hexadecapole H_z^α. It shows an eight-fold symmetry with a $\pi/8$ phase shift between the $\sigma\pi$ and $\sigma\sigma$ channels. The peak intensity of the $\sigma\sigma$ channel is about 2 orders of magnitude larger than that of the $\sigma\pi$ channel. The eight-fold symmetry is a characteristic of this H_z^α hexadecapolar OP. Fig. 2(c,d) shows the results of the A_{2-} dipole J_z and octupole T_z^α. It shows a nonzero constant in the $\sigma\pi$ channel and no signal in the $\sigma\sigma$ channel. Fig. 2(e,f) displays the results of the B_{1+} quadrupole O_{22} and hexadecapole O_{42}. It shows a d_{xy} wave pattern in the $\sigma\pi$ channel and $d_{x^2-y^2}$ wave pattern in the $\sigma\sigma$ channel. In Fig. 2(g,h) the results of B_{1-} octupole T_{xyz} shows a d_{xy} wave pattern in the $\sigma\pi$ channel and no signal in the $\sigma\sigma$ channel. Fig. 2(i,j) plots the results of B_{2+} quadrupole O_{xy} and hexadecapole H_z^β exhibiting a $d_{x^2-y^2}$ wave pattern in the $\sigma\pi$ channel and d_{xy} pattern in the $\sigma\sigma$ channel. Finally, the results of the B_{2-} octupole T_z^β are shown in Fig. 2(k,l) where a $d_{x^2-y^2}$ wave pattern is seen in the $\sigma\pi$ channel and nothing is seen in the $\sigma\sigma$ channel. In general, we find that there are no signals in $\sigma\sigma$ channel for time-reversal broken OPs. The azimuthal dependence show different symmetries for different multipole, so it can be used to distinguish multipolar OPs.

B. REXS Results

The body centered tetragonal structure of URu_2Si_2 forbids Bragg peaks with $H+K+L=2n+1$. We infer that the HO state breaks the body centered symmetry by creating inequivalent U sites, thus allowing Bragg peaks at these once forbidden positions. We performed an extensive search for HO Bragg peaks along $(0,0,L)$ and $(1,0,L)$ directions; results for the former are displayed in Fig. 3. Broad peaks are observed at $(0,0,2n+1)$. However, these peaks persist through the phase transition at T_{HO}, strongly suggesting that these are not related to the HO phase. Additionally, no resonance enhancement is observed across the U L_3 edge. This suggests that the HO is not accessible through the $E1$ or $E2$ transitions using experiments of this type. These results are consistent with former studies[40,41] in which no quadrupolar OPs are found. However, we still cannot exclude the possibility of octupole and hexadecapole due to the weak signal of the $E2$ transition.

Despite our negative result in the search for the HO, additional experiments are needed to definitely prove the existence (or absence) of the octupole or hexadecapole OPs. Designing experimental techniques to enhance the sensitivity to the $E2$ transition at U-L_3 edge is needed to observe higher rank multipoles. One of such techniques is the Borrmann spectroscopy[50,51]. The Borrmann effect refers to the anomalous transmission of X-rays through very perfect single-crystal slabs when they are in symmetric Laue diffraction condition[50]. This effect can be interpreted by the theory of dynamical diffraction of X-rays[50]. It is a consequence of multiple coherent interference of the incident and diffracted beams which produces a total electric field with almost zero amplitude but largely enhanced gradient at the crystal planes. The dipolar transition is thus suppressed because it is proportional to the amplitude of the electric field and, on the contrary, the quadrupolar transition will be largely enhanced because it is proportional to the gradient of the electric field. Therefore, we may have a chance to detect strong quadrupolar signal, for example at U-L_3 edge. In Ref. 51, Pettifer *et al.* indeed observed very

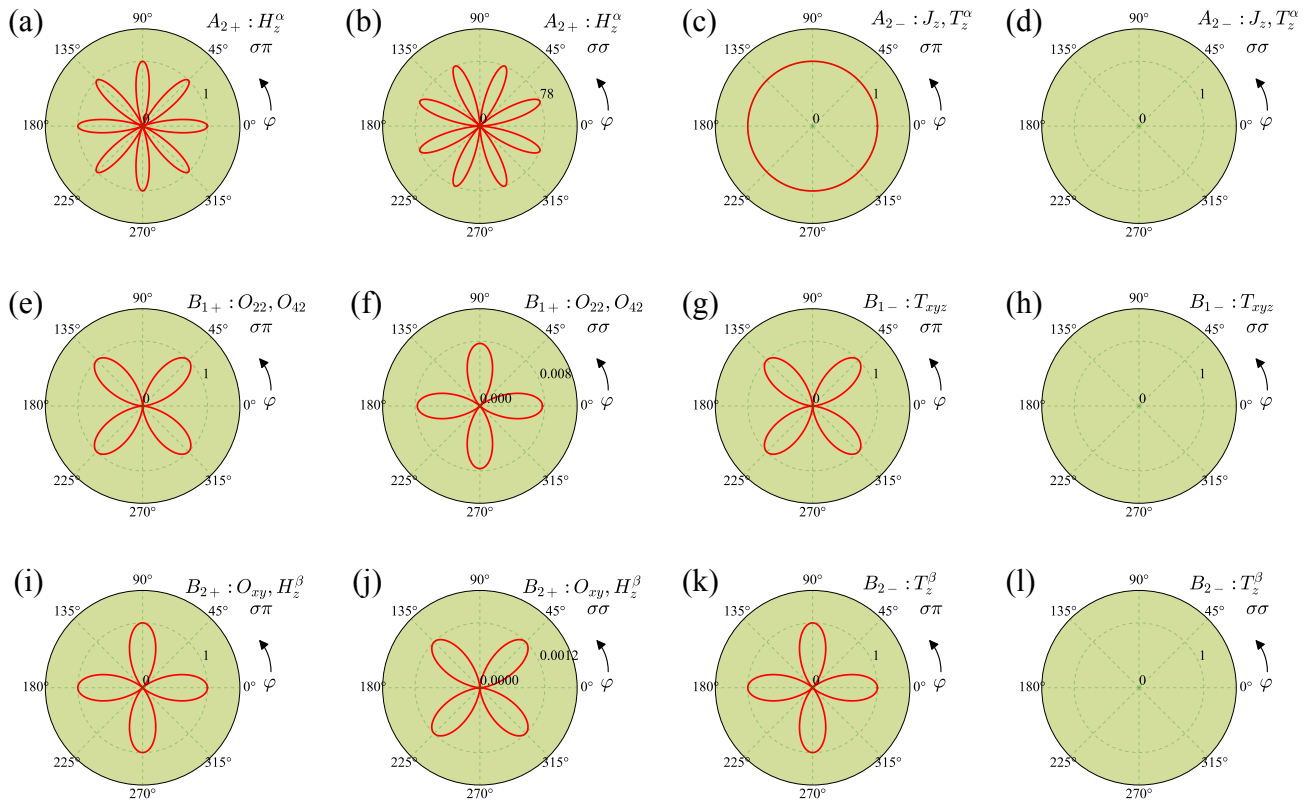

FIG. 2. (Color online). The calculated azimuthal dependence of a $(0,0,3)$ reflection of L_3-$E2$ transition in both $\sigma\pi$ and $\sigma\sigma$ channels for different proposals of multipolar OPs. The incident photon energy is 17.167 keV and the azimuthal angle is defined with respect to [100] direction. For each proposal, the intensity is normalized by the maximum intensity of its $\sigma\pi$ channel. (a,b) A_{2+} hexadecapole H_z^α, (c,d) A_{2-} dipole J_z and ocutpole T_z^α, (e,f) B_{1+} quadrupole O_{22} and hexadecapole O_{42}, (g,h) B_{1-} octupole T_{xyz}, (i,j) B_{2+} quadrupole O_{xy} and hexadecapole H_z^β, (k,l) B_{2-} octupole T_z^β.

strong quadrupolar peak in the absorption spectrum at L_1, L_2 and L_3 edges of Gadolinium in a $4f$ compound gadolinium gallium garnet. However, no results of $5f$ compounds have been reported, so it is worth to try in $5f$ compounds, such as URu_2Si_2. Borrmann spectroscopy requires samples that are much thicker than the nominal X-ray penetration depth and sufficiently perfect that at least some x-rays can transmit through the sample without encountering defects, which may be a challenge for sample growth.

Polarization analysis of the outgoing X-rays can also be advantageous (despite the strong reduction in X-ray throughput that it imposes) because, as we will demonstrate, the HO Bragg peak should be observed in the $\sigma\pi$ channel. Additionally, identifying the energy and cross-section of the L_3- $E2$ transition will greatly facilitate the search for superlattice peaks.

C. Intensity estimation of the L_3-$E2$ transition

We further justify the negative experimental results by estimating the intensity of the L_3-$E2$ transition. Usually, the intensity of the $E2$ transition will be much weaker than that of the $E1$ transition. This is mainly caused by the very small overlap integral of r^2 between the core hole and valence orbitals. Thus, it is critical to give an estimation of the relative intensity of the L_3-$E2$ transition compared with known experiments which have strong intensity, such as the M_4-$E1$ transition. Roughly, the relative intensity between L_3-$E2$ and M_4-$E1$ is,

$$\frac{I(L_3-E2)}{I(M_4-E1)} \propto \left(\frac{k}{3}\frac{\omega_{L_3}}{\omega_{M_4}}\frac{\langle 2p\,|\,r^2\,|\,5f\rangle}{\langle 3d\,|\,r\,|\,5f\rangle}\right)^4 \left(\frac{\Gamma_{M_4}}{\Gamma_{L_3}}\right)^2, \tag{32}$$

and that between L_3-$E2$ and L_3-$E1$ is,

$$\frac{I(L_3-E2)}{I(L_3-E1)} \propto \left(\frac{k}{3}\frac{\langle 2p\,|\,r^2\,|\,5f\rangle}{\langle 2p\,|\,r\,|\,6d\rangle}\right)^4, \tag{33}$$

where, ω_{L_3} and ω_{M_4} are the X-ray frequency of the L_3 and M_4 edges, their ratio is about 4.6. Based on the HF calculations, the overlap integral ratio $\langle 2p\,|\,r^2\,|\,5f\rangle / \langle 3d\,|\,r\,|\,5f\rangle \approx 0.013$ and $\langle 2p\,|\,r^2\,|\,5f\rangle / \langle 2p\,|\,r\,|\,6d\rangle \approx 0.2$, respectively. Γ_{M_4} and

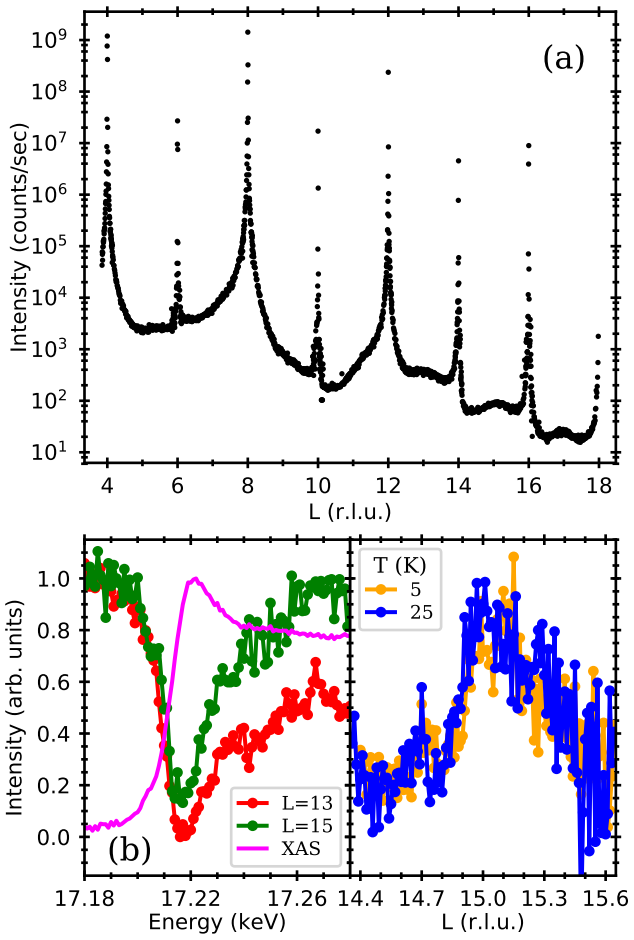

FIG. 3. (a) X-ray diffraction L dependence measured along $(0,0,L)$ direction using 17.215 keV and $\varphi = 1.2°$. (b) Energy dependence of (0,0,13) and (0,0,15) Bragg peaks together with the U L_3 edge XANES. (c) Temperature dependence of (0,0,15) Bragg peak.

Γ_{L_3} are the core-hole lifetime width for M_4 and L_3 edge, respectively, and their ratio is $\Gamma_{M_4}/\Gamma_{L_3} \approx 0.4$. For the L_3 edge, $k/3 \approx 2.9$. Thus, the intensity of L_3-$E2$ is about 10^{-4} times smaller than that of M_4-$E1$ and 10^{-1} times smaller than that of L_3-$E1$. Here, we should note that $6d$ orbitals are much broader in URu_2Si_2, which will lead to larger overlap integrals than those based on the atomic $6d$ orbitals, so L_3-$E2$ is not just one order of magnitude smaller than that of L_3-$E1$. We may expect larger overlap integrals for the M_3-$E2$ ($3p_{3/2} \rightarrow 5f$) transition, so we also calculate the relative intensity between M_3-$E2$ and M_4-$E1$. The results show that the intensity of M_3-$E2$ is also about 10^{-4} times smaller than that of M_4-$E1$. The reason is that, although the calculated overlap integral $\langle 3p \,|\, r^2 \,|\, 5f \rangle$ is about 14 times larger than that of $\langle 2p \,|\, r^2 \,|\, 5f \rangle$, both of the X-ray frequency and wavevector of M_3 edge is about 0.25 times smaller than that of L_3 edge, as a result, the enhancement effect from the larger overlap integral is cancelled out. The intensity of M_3-$E2$ is not stronger than that of L_3-$E2$.

However, this rough estimation does not consider many details of the scattering process, such as the ground state and the intermediate excited states, the interference effects of intermediate states, the smearing effect of core-hole lifetime width and the geometry of the experimental setup. To give a better estimation, we exactly diagonalize the atomic ground and excited Hamiltonians to get the eigenstates and the transition matrix, and then we choose different ground states and experimental geometries to calculate the cross section according to Eqn. 1 and Eqn. 2.

The calculated results of a $(0,0,3)$ reflection are shown in Fig. 4. The azimuthal angle φ is defined with respect to the [100] direction and the polarization of outgoing light is not analyzed. We plot both the σ and π polarizations of the incident light. The difference of energy levels between $6d$ and $5f$ is set to be 10 eV. We assume a type-I antiferro-multipolar order with $Q_{AF} = (0,0,1)$ in the simulation. Fig. 4(a,b,c) are the results for the ground state (Eqn. 29) that induces A_{2-} orders: dipole J_z and octupole T_z^α. The $E1$ transition can only detect J_z but $E2$ can detect both of them. The azimuthal angle is set to be $\varphi = 0$. For this ground state, the intensity of L_3-$E2$ is about 10^{-6} times smaller than that of M_4-$E1$. However, the intensity of L_3-$E2$ is almost the same order of magnitude as that of L_3-$E1$ transition. In Fig. 4(c), the left peak is from the $E2$ transition and the right peak is from the $E1$ transition. Fig. 4(d,e,f,g,h,i) plots the results for the ground state (Eqn. 31) that induces B_{2+} order: quadrupole O_{xy} and hexadecapole H_z^β. In Fig. 4(d,e,f) the azimuthal angle is $\varphi = 0$. We find that the intensity of L_3-$E2$ transition is 10^{-5} times smaller than that of M_4-$E1$ transition and has the same order of magnitude as that of L_3-$E1$. In Fig. 4(g,h,i), the azimuthal angle is set to be $\varphi = \pi/4$. For σ polarization, the intensity of L_3-$E2$ is about 10^{-9} times smaller than that of M_4-$E1$ and 10^{-5} smaller than that of L_3-$E1$. However, for π polarization, it is only 10^{-5} times smaller than that of M_4-$E1$ and much larger than that of L_3-$E1$ so that there is only a $E2$ peak. Fig. 4(j) is the result for the ground state (Eqn. 31) that induces B_{2-} octupolar order T_z^β. The intensity is at least 8 order of magnitude smaller than that of M_4-$E1$. Another B_{1-} octupole T_{xyz} has the same order of magnitude as that of T_z^β. Fig. 4(k,l) are the results for the ground state (Eqn. 29) that induces the A_{2+} hexadecapolar order H_z^α. For $\varphi = 0$, both σ and π polarizations are at least 7 order of magnitude smaller than that of M_4-$E1$. For $\varphi = \pi/8$, σ polarization is about 5 order of magnitude smaller than that of M_4-$E1$. We emphasize that the atomic calculation underestimate the intensity of L_3-$E1$ transition due to the itinerant character of $6d$ orbitals, so the intensity of L_3-$E1$ should be much larger than that of L_3-$E2$ in reality.

Based on these atomic results, we find that there are many factors that will affect the REXS cross-section, such as the interference of the intermediate states, the interference effect of core-hole lifetime width, the exper-

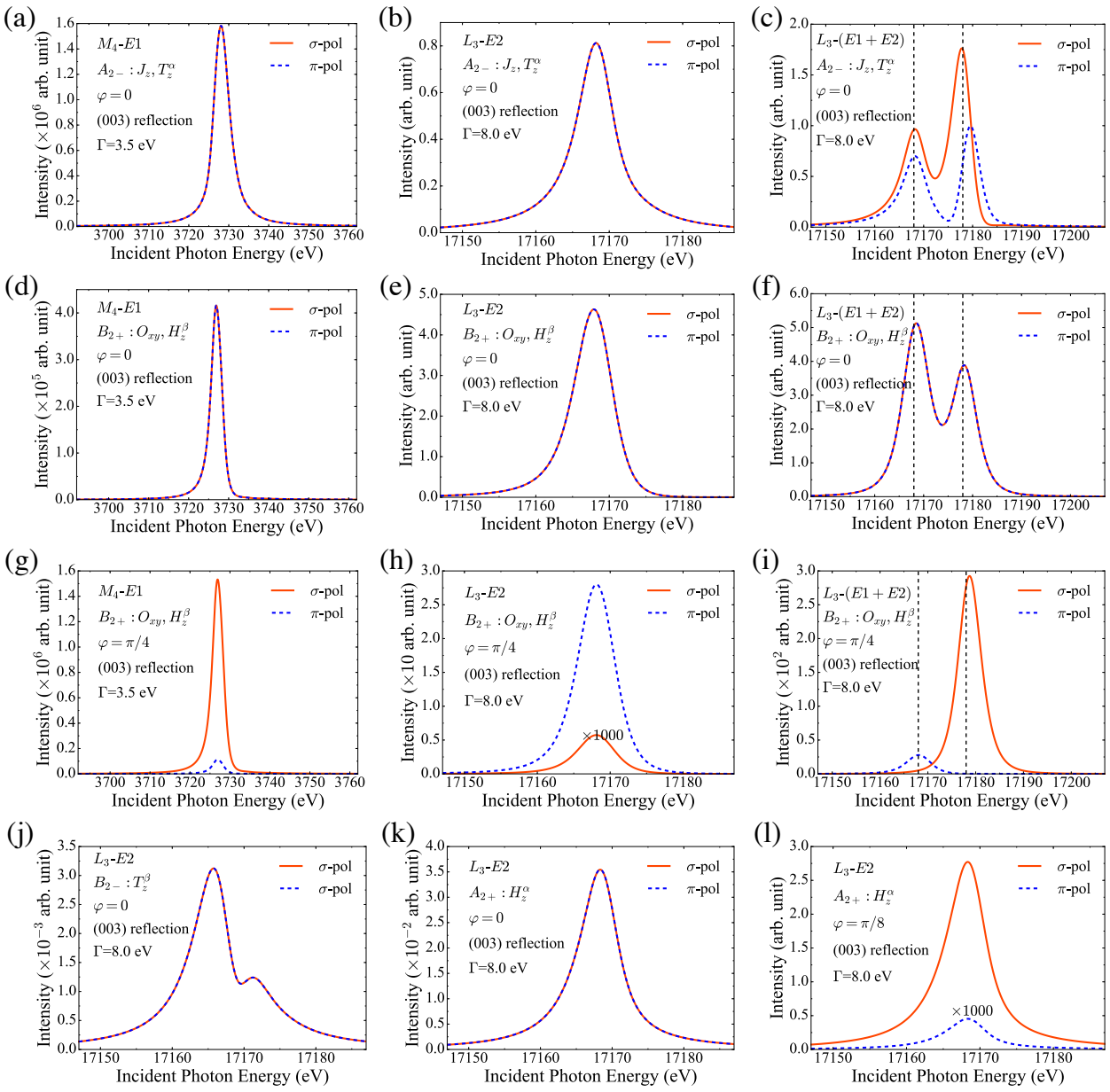

FIG. 4. (Color online). $(0,0,3)$ REXS intensity as a function of incident photon energy and polarization. The incoming light is linearly polarized and the polarization of the outgoing light is not analyzed. We compare the results of the M_4-$E1$ transition with the L_3-$E2$ transition and the L_3-$(E1+E2)$ transition. We consider different ordering schemes: (a,b,c) Antiferro-dipole J_z and antiferro-octupole T_z^α at $\varphi = 0$. (d,e,f) Antiferro-quadrupole O_{xy} and antiferro-hexadecapole H_z^β at $\varphi = 0$. (g,h,i) Antiferro-quadrupole O_{xy} and antiferro-hexadecapole H_z^β at $\varphi = \frac{\pi}{4}$. (j) Antiferro-octupole T_z^β at $\varphi = 0$. (k) Antiferro-hexadecapole H_z^α at $\varphi = 0$. (l) Antiferro-hexadecapole H_z^α at $\varphi = \pi/8$.

imental geometry and the details of the ground states. Overall, the intensity of L_3-$E2$ transition is at least 5 or 6 orders of magnitude smaller than that of M_4-$E1$, so the signal of L_3-$E2$ transition is indeed very weak compared with M_4-$E1$. We also note that the $5f$ electrons are not completely localized and they have partial itinerant character in URu_2Si_2, which leads to the importance of the band effects in the REXS cross-section. To account for these effects, the combination of more advanced first-principle calculations, such as density functional theory plus dynamical mean-field theory (DFT+DMFT), with REXS cross-section calculations is needed. Despite this, the simple atomic simulations still give us preliminary estimations about the strength of the $E2$ transition.

To further confirm the weakness of L_3-$E2$ signal, we estimate the flux of the scattered photons by cal-

culating the absolute value of the cross-section. For a typical flux of 10^{11}ph/s/100meV/$(100 \times 100\mu m^2)$, a rough upper bound of the flux of scattered photon is 10^4ph/s/eV/rad for M_4-$E1$ transition, while it is $10^{-1} \sim 10^{-2}$ph/s/eV/rad for L_3-$E2$ transition. This makes it very difficult to be detected in experiments, which is consistent with the experimental results.

IV. SUMMARY

In summary, we have studied the possibility to detect multipolar OPs in URu_2Si_2 by REXS in the U L_3-$E2$ transition channel. The REXS experiments do not find any clear signal indicating multipolar OPs. An estimation based on atomic calculations indicates that the intensity of the L_3-$E2$ transition is indeed much smaller than that of M_4-$E1$ transition and the flux of the scattered photons is too small such that it is very difficult to detect the $E2$ signal. It seems that it is still not practical to use the $E2$ transition of currently available REXS experiment to detect the multipolar OPs. Developing experimental techniques to enhance $E2$ signal is urgently needed to identify the multipolar OPs not only in URu_2Si_2 but also in other compounds, such as UO_2, NpO_2 and $Ce_{1-x}La_xB_6$[52].

V. ACKNOWLEDGMENTS

We thank Frank de Groot for valuable discussions. This work was supported by the U.S. Department of energy, Office of Science, Basic Energy Sciences as a part of the Computational Materials Science Program. G.F. and D.M. were supported by the U.S. Department of Energy, Office of Science, Office of Basic Energy Sciences, under Contract No. DE-SC00112704, and Early Career Award Program under Award No. 1047478. X.L. is supported by MOST (Grant No.2015CB921302) and CAS (Grant No. XDB07020200). This research used resources of the Advanced Photon Source, a U.S. Department of Energy (DOE) Office of Science User Facility operated for the DOE Office of Science by Argonne National Laboratory under Contract No. DE-AC02-06CH11357. Work at Los Alamos National Laboratory was performed under the auspices of the U.S. Department of Energy, Office of Basic Energy Sciences, Division of Materials Sciences and Engineering.

Appendix A: Slater integrals and spin-orbit coupling parameters

TABLE I. Slater integrals and spin-orbit coupling parameters for ground configuration $5f^2$ (in eV).

F^0_{ff}	F^2_{ff}	F^4_{ff}	F^6_{ff}	ζ_{5f}
0.291	7.611	4.979	3.655	0.261

TABLE II. Slater integrals and spin-orbit coupling parameters for excited configuration $2p^55f^3$ (in eV).

F^0_{ff}	F^2_{ff}	F^4_{ff}	F^6_{ff}	F^0_{pf}	F^2_{pf}	G^2_{pf}	G^4_{pf}
0.306	7.984	5.232	3.845	0.005	0.497	0.082	0.053
ζ_{5f}	ζ_{2p}						
0.302	2517.292						

TABLE III. Slater integrals and spin-orbit coupling parameters for excited configuration $2p^55f^26d^1$ (in eV).

F^0_{ff}	F^2_{ff}	F^4_{ff}	F^6_{ff}	F^0_{pf}	F^2_{pf}	G^2_{pf}	G^4_{pf}
0.307	8.278	5.447	4.011	0.102	0.528	0.087	0.056
F^0_{pd}	F^2_{pd}	G^1_{pd}	G^3_{pd}	F^0_{fd}	F^2_{fd}	F^4_{fd}	G^1_{fd}
0.022	0.272	0.238	0.142	0.139	3.750	2.050	1.938
G^3_{fd}	G^5_{fd}	ζ_{5f}	ζ_{6d}	ζ_{2p}			
1.562	1.213	0.321	0.435	2517.236			

TABLE IV. Slater integrals and spin-orbit coupling parameters for excited configuration $3d^55f^3$ (in eV).

F^0_{ff}	F^2_{ff}	F^4_{ff}	F^6_{ff}	F^0_{df}	F^2_{df}	F^4_{df}
0.307	8.020	5.258	3.865	0.102	2.051	0.952
G^1_{df}	G^3_{df}	G^5_{df}	ζ_{5f}	ζ_{3d}		
1.602	0.969	0.678	0.301	70.449		

[1] T. T. M. Palstra, A. A. Menovsky, J. v. d. Berg, A. J. Dirkmaat, P. H. Kes, G. J. Nieuwenhuys, and J. A. Mydosh, Phys. Rev. Lett. **55**, 2727 (1985).
[2] C. Broholm, J. K. Kjems, W. J. L. Buyers, P. Matthews, T. T. M. Palstra, A. A. Menovsky, and J. A. Mydosh, Phys. Rev. Lett. **58**, 1467 (1987).
[3] C. Broholm, H. Lin, P. T. Matthews, T. E. Mason, W. J. L. Buyers, M. F. Collins, A. A. Menovsky, J. A. Mydosh, and J. K. Kjems, Phys. Rev. B **43**, 12809 (1991).
[4] D. E. MacLaughlin, D. W. Cooke, R. H. Heffner, R. L. Hutson, M. W. McElfresh, M. E. Schillaci, H. D. Rempp, J. L. Smith, J. O. Willis, E. Zirngiebl, C. Boekema, R. L. Lichti, and J. Oostens, Phys. Rev. B **37**, 3153 (1988).
[5] H. Amitsuka, K. Matsuda, I. Kawasaki, K. Tenya, M. Yokoyama, C. Sekine, N. Tateiwa, T. Kobayashi, S. Kawarazaki, and H. Yoshizawa, Journal of Magnetism and Magnetic Materials **310**, 214 (2007).
[6] H. Amitsuka, M. Sato, N. Metoki, M. Yokoyama, K. Kuwahara, T. Sakakibara, H. Morimoto, S. Kawarazaki, Y. Miyako, and J. A. Mydosh, Phys. Rev. Lett. **83**, 5114 (1999).
[7] N. P. Butch, J. R. Jeffries, S. Chi, J. B. Leão, J. W. Lynn, and M. B. Maple, Phys. Rev. B **82**, 060408 (2010).
[8] P. Santini and G. Amoretti, Phys. Rev. Lett. **73**, 1027 (1994).
[9] P. Santini, Phys. Rev. B **57**, 5191 (1998).
[10] F. J. Ohkawa and H. Shimizu, Journal of Physics: Condensed Matter **11**, L519 (1999).
[11] P. Santini, G. Amoretti, R. Caciuffo, F. Bourdarot, and B. Fåk, Phys. Rev. Lett. **85**, 654 (2000).
[12] A. Kiss and P. Fazekas, Phys. Rev. B **71**, 054415 (2005).
[13] K. Hanzawa, Journal of Physics: Condensed Matter **19**, 072202 (2007).
[14] K. Haule and G. Kotliar, Nat. Phys. **5**, 796 (2009).
[15] F. Cricchio, F. Bultmark, O. Grånäs, and L. Nordström, Phys. Rev. Lett. **103**, 107202 (2009).
[16] H. Harima, K. Miyake, and J. Flouquet, Journal of the Physical Society of Japan **79**, 033705 (2010).
[17] H. Kusunose and H. Harima, Journal of the Physical Society of Japan **80**, 084702 (2011).
[18] H. Ikeda, M. Suzuki, R. Arita, T. Takimoto, T. Shibauchi, and Y. Matsuda, Nat. Phys. **8**, 528 (2012).
[19] M. B. Maple, J. W. Chen, Y. Dalichaouch, T. Kohara, C. Rossel, M. S. Torikachvili, M. W. McElfresh, and J. D. Thompson, Phys. Rev. Lett. **56**, 185 (1986).
[20] H. Ikeda and Y. Ohashi, Phys. Rev. Lett. **81**, 3723 (1998).
[21] V. P. Mineev and M. E. Zhitomirsky, Phys. Rev. B **72**, 014432 (2005).
[22] J. G. Rau and H.-Y. Kee, Phys. Rev. B **85**, 245112 (2012).
[23] L. P. Gor'kov and A. Sokol, Phys. Rev. Lett. **69**, 2586 (1992).
[24] P. Chandra, P. Coleman, J. A. Mydosh, and V. Tripathi, Nature **417**, 831 (2002).
[25] C. M. Varma and L. Zhu, Phys. Rev. Lett. **96**, 036405 (2006).
[26] S. Elgazzar, J. Rusz, M. Amft, P. M. Oppeneer, and J. A. Mydosh, Nat Mater **8**, 337 (2009).
[27] S. Fujimoto, Phys. Rev. Lett. **106**, 196407 (2011).
[28] Y. Dubi and A. V. Balatsky, Phys. Rev. Lett. **106**, 086401 (2011).
[29] P. Chandra, P. Coleman, and R. Flint, Nature **493**, 621 (2013).
[30] P. Chandra, P. Coleman, and R. Flint, Phys. Rev. B **91**, 205103 (2015).
[31] J. A. Mydosh and P. M. Oppeneer, Rev. Mod. Phys. **83**, 1301 (2011).
[32] J. Mydosh and P. Oppeneer, Philosophical Magazine **94**, 3642 (2014).
[33] J. Buhot, M.-A. Méasson, Y. Gallais, M. Cazayous, A. Sacuto, G. Lapertot, and D. Aoki, Phys. Rev. Lett. **113**, 266405 (2014).
[34] H.-H. Kung, R. E. Baumbach, E. D. Bauer, V. K. Thorsmølle, W.-L. Zhang, K. Haule, J. A. Mydosh, and G. Blumberg, Science **347**, 1339 (2015), http://science.sciencemag.org/content/347/6228/1339.full.pdf.
[35] H.-H. Kung, S. Ran, N. Kanchanavatee, V. Krapivin, A. Lee, J. A. Mydosh, K. Haule, M. B. Maple, and G. Blumberg, Phys. Rev. Lett. **117**, 227601 (2016).
[36] L. J. P. Ament, M. van Veenendaal, T. P. Devereaux, J. P. Hill, and J. van den Brink, Reviews of Modern Physics **83**, 705 (2011).
[37] T. Matsumura, H. Nakao, and Y. Murakami, Journal of the Physical Society of Japan **82**, 021007 (2013).
[38] E. D. Isaacs, D. B. McWhan, R. N. Kleiman, D. J. Bishop, G. E. Ice, P. Zschack, B. D. Gaulin, T. E. Mason, J. D. Garrett, and W. J. L. Buyers, Phys. Rev. Lett. **65**, 3185 (1990).
[39] T. Nagao and J. ichi Igarashi, Journal of the Physical Society of Japan **74**, 765 (2005).
[40] H. Amitsuka, T. Inami, M. Yokoyama, S. Takayama, Y. Ikeda, I. Kawasaki, Y. Homma, H. Hidaka, and T. Yanagisawa, Journal of Physics: Conference Series **200**, 012007 (2010).
[41] H. C. Walker, R. Caciuffo, D. Aoki, F. Bourdarot, G. H. Lander, and J. Flouquet, Phys. Rev. B **83**, 193102 (2011).
[42] R. D. dos Reis, L. S. I. Veiga, D. Haskel, J. C. Lang, Y. Joly, F. G. Gandra, and N. M. Souza-Neto, (2016), arXiv:1601.02443 [cond-mat.str-el].
[43] T. Nagao and J.-i. Igarashi, Phys. Rev. B **74**, 104404 (2006).
[44] R. D. Cowan, *The Theory of Atomic Structure and Spectra* (University of California Press, Berkeley, 1981).
[45] P. H. Butler, *Point Group Symmetry Applications: Methods and Tables* (Plenum Press, New York, 1981).
[46] F. D. Groot and A. Kotani, *Core level spectroscopy of solids* (CRC press, 2008).
[47] E. Stavitski and F. M. de Groot, Micron **41**, 687 (2010).
[48] M. Sundermann, M. W. Haverkort, S. Agrestini, A. Al-Zein, M. Moretti Sala, Y. Huang, M. Golden, A. de Visser, P. Thalmeier, L. H. Tjeng, and A. Severing, Proceedings of the National Academy of Sciences (2016), 10.1073/pnas.1612791113.
[49] T. D. Matsuda, D. Aoki, S. Ikeda, E. Yamamoto, Y. Haga, H. Ohkuni, R. Settai, and Y. Onuki, J. Phys. Soc. Japan **77**, 362 (2008).
[50] B. W. Batterman and H. Cole, Rev. Mod. Phys. **36**, 681 (1964).
[51] R. F. Pettifer, S. P. Collins, and D. Laundy, Nature **454**, 196 (2008).
[52] P. Santini, S. Carretta, G. Amoretti, R. Caciuffo, N. Magnani, and G. H. Lander, Rev. Mod. Phys. **81**, 807 (2009).